ADVANCED FUNCTIONAL MATERIALS
www.afm-journal.de

Location, Location, Location - Strategic Positioning of 2,1,3-Benzothiadiazole Units within Trigonal Quaterfluorene-Truxene Star-Shaped Structures

Colin R. Belton, Alexander L. Kanibolotsky, James Kirkpatrick, Clara Orofino, Saadeldin E. T. Elmasly, Paul N. Stavrinou, Peter J. Skabara, and Donal D. C. Bradley**

The fused, bicyclic molecule, 2,1,3-Benzothiadiazole (BT), has become a key ingredient in the design of new organic semiconductors for light emission and energy harvesting applications. Here, the synthesis is reported of a series of trigonal, star-shaped compounds comprising a truxene core and three quater-dialkylfluorene arms into each of which a BT unit is inserted sequentially at each possible position (T4BT-A to T4BT-E). Analysis of the resulting electronic properties shows that as a consequence of conjugative coupling to the core and the resulting symmetry there are three distinct locations for the BT unit and the influence that these locations have on light emission and other spectroscopic characteristics is discussed. The systematic variation in photophysical properties for the different structural isomers helps to clarify the influence of BT unit addition to 9,9-dialkylfluorene chains. It also helps to establish a design template for the construction of donor-acceptor conjugated materials with targeted properties. For T4BT-E with a BT unit at the terminal position of each arm, the photoluminescence quantum efficiency is significantly reduced and no amplified spontaneous emission is observed under typical pumping conditions. Theoretical calculations assist in understanding the variation in behaviors among the T4BT-X family of compounds, especially in relation to their photoluminescence decay times and the Raman scattering intensities of their dominant BT-unit-centred molecular vibrations.

1. Introduction

One of the great strengths of organic electronics is the possibility of chemically tuning materials to produce new compounds tailored for specific applications. Organic light emitting diodes (OLEDs) have been the first devices to be commercialized, featuring in highly regarded active matrix (AMOLED) mobile phone displays. The pursuit of solution-processed approaches to these applications has given rise to the design and synthesis of complex materials incorporating a variety of chemical moieties and chain architectures to enhance charge injection and transport, emission efficiency and color definition, and device lifetime and manufacturability.[1–3] Large area passive matrix structures for lighting or optical gain structures for amplification and lasing represent, in many ways, even more challenging targets for these complex emission materials.[4] In the latter case, it should be noted that not all materials that show good performance in OLEDs show efficient optical gain at low pump thresholds.[5] Working with well-defined chemical systems helps to better understand the requirements and this has motivated our development of star-shaped molecules composed of a central truxene unit from which emanate three short conjugated arms. We have previously reported on the properties of blue light emission mono-, bi-, ter- and quater-dialkylfluorene (**T1**-**T4**) arm/ truxene core compounds.[6,7] We have also previously reported detailed studies of related hexa-dialkylfluorene substituted truxene/triazatruxene core and tetra-dialkylfluorene substituted pyrene core compounds, including OLED, optical gain, and lasing performance.[8] These previous studies have allowed us to investigate the influence of arm length, arm number and core type from among a wide range of star-shaped molecule parameters. We now report (**Figure 1**) novel **T4**-based structures where fused bicyclic 2,1,3-benzothiadiazole (BT) units are sequentially inserted at each of the five possible positions within the quater-dialkylfluorene arms. This yields compounds **T4BT-A**, **T4BT-B**, **T4BT-C**, **T4BT-D** and **T4BT-E**, beginning with BT adjacent to the truxene core (**T4BT-A**) and moving this unit

Dr. C. R. Belton, Dr. P. N. Stavrinou, Prof. D. D. C. Bradley
Department of Physics and Centre for Plastic Electronics
Imperial College London
South Kensington Campus, London SW7 2BZ, UK
E-mail: d.bradley@imperial.ac.uk
Dr. A. L. Kanibolotsky, C. Orofino, S. E. T. Elmasly, Prof. P. J. Skabara
WestCHEM, Department of Pure and Applied Chemistry
University of Strathclyde
295 Cathedral Street, Glasgow G1 1XL, UK
E-mail: peter.skabara@strath.ac.uk
Dr. A. L. Kanibolotsky
Institute of Physical Organic Chemistry and Coal Chemistry
83114, Donetsk, Ukraine
Dr. J. Kirkpatrick
Mathematical Institute
University of Oxford
24-29 St Giles', Oxford OX1 3LB, UK

DOI:10. 1002/adfm.201202644

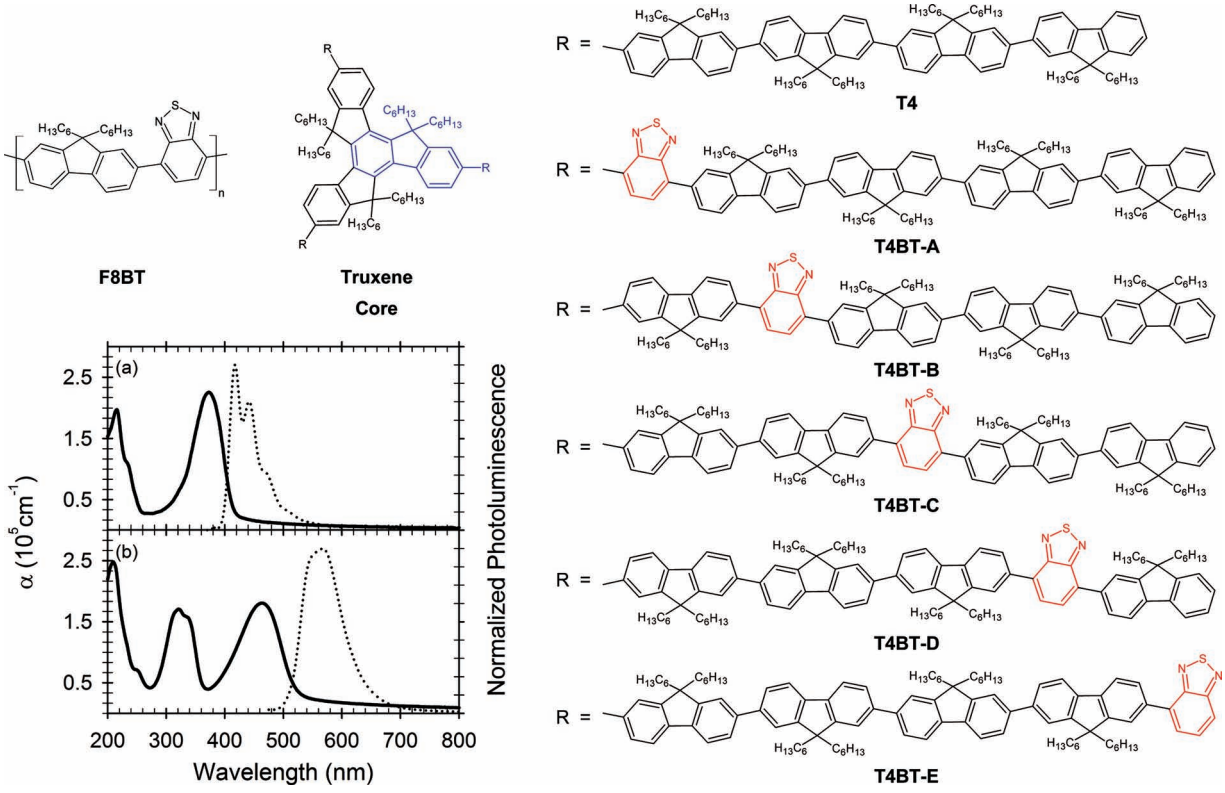

Figure 1. Chemical structures of truxene-cored star-shaped compounds **T4BT-A**, **-B**, **-C**, **-D** and **-E**, the parent **T4** truxene and the alternating copolymer **F8BT**. The highlighted part of the truxene core (blue) identifies an effective 9,9-dihexylfluorene unit to which the attached arm is conjugatively coupled. BT units are highlighted in red. Also shown for reference are the absorption (solid lines) and PL (dotted lines) for the **T4** truxene (panel (a)) and **F8BT** polymer (panel (b)).

stepwise to position the heterocycle at the termini of the arms (**T4BT-E**). The development of these compounds represents the introduction of an additional degree of freedom into the design of star-shaped molecules.[9]

The BT unit is a fascinating fused heterocycle that was first introduced into fluorene-based copolymer light emitting diode material systems by E. P. Woo and colleagues at the Dow Chemical Company.[10] It has been used since to great effect in the design of new organic semiconductors for light emission and energy harvesting applications. If it is embedded in simple conjugated structures, BT's electron-deficient character serves to stabilize and spatially localize the lowest unoccupied molecular orbital (LUMO).[11] This has allowed the generation of efficient copolymer green emission materials, such as poly(9,9-dioctylfluorene-co-benzothiadiazole) (**F8BT** see Figure 1)[12,13] with advantageously lowered electron injection barriers.[14,15] Subsequent optimization for OLEDs has been achieved by blending **F8BT** with poly(9,9-dioctylfluorene) (PFO) and/or fluorene-arylamine copolymers, the latter with advantageously lowered hole injection barriers.[16,17] The final step has been to make complex copolymers containing a mixture of BT, arylamine and fluorene constituents, as for example found in the proprietary Lumation green and other polymers.[18,19]

Red emission materials can also be achieved by linking BT with thiophene-based structures. The three-component thiophene-benzothiadiazole-thiophene chromophore is a particularly common structure in this regard, again one that was introduced by the Dow Chemical Company in their development of red emission fluorene copolymers, like Dow Red F and more recent proprietary Lumation red materials.[14,20–22] The three-component thiophene-benzothiadiazole-thiophene sequence is also used in a variety of energy harvesting materials for solar cells including the well-known poly[2,6-(4,4-bis-(2-ethylhexyl)-4*H*-cyclopenta[2,1-*b*;3,4-*b*']-dithiophene)-*alt*-4,7-(2,1,3-benzothiadiazole) (PCDTBT) polymer.[23] BT has, moreover, been combined with other thiophene based units to achieve smaller optical gap solar cell polymers and molecular light absorbers for dye-sensitized solar cells.[24–27]

A greater understanding of the electronic interplay between the BT and neighboring units in a given structure would be highly beneficial to the organic electronics community - particularly at the most fundamental level in the structural design of new semiconductors. To this end, the series of structural isomers **T4BT-A** to **T4BT-E** allows a thorough investigation of the effect of subtle variations in environment on the influence of BT addition to a 9,9-dialkylfluorene chain. Importantly, unlike 9,9-dialkylfluorene/BT copolymer studies with varying fractions of BT inclusion[28] the molecular architecture here is precisely defined; each of the isomers can be studied as a separate entity. In the copolymers, the distribution of BT units within each chain in a sample is much less well defined and subtle effects

will then be averaged out over the ensemble. The trigonal structure also provides a defined symmetry that helps us to explain the observed electronic properties. Our **T4BT-X** series are, moreover, highly efficient green emitters with excellent solubility and film-forming properties. The new materials have been characterized by absorption, emission (photoluminescence (PL) and amplified spontaneous emission (ASE)) and Raman spectroscopy. Symmetry plays an important role for absorption and PL spectra with a pair-wise equivalence of the **T4BT-A** and **-D** and **T4BT-B** and **-C** structures. **T4BT-E** represents a distinct situation where placement of the BT unit at the terminal position of the quater(9,9-dialkylfluorene) arm leads to significant alterations in behavior. It is these two pairs and the terminal position that represent the three *locations* of the paper title (see also the table of contents graphic).

As shown below, however, a more detailed description is needed to explain the subtle trends in Raman intensity for BT-centred vibrations at ≈ 1360 and ≈ 1547 cm^{-1} and in PL decay times. Density functional theory/time dependent density functional theory (DFT/TD-DFT) calculations match well to the experimental results for Raman intensity and also do a very fair job of predicting the oscillator strengths for the longest wavelength (≈455 nm) absorption peak without requiring any variation in torsional angle for the BT unit. The key factor is the distribution of the HOMO/occupied Natural Transition Orbital (NTO) amplitude along the arm and specifically the proportion of the wavefunction present on the BT unit. PL decay times are harder to rationalize and one has to factor in the influence of non-radiative decay processes. The precision in the chemical structure of these compounds relative to 9,9-dialkylfluorene/BT copolymers allows a consideration of the role of BT location in isolation from other factors; there is no ensemble averaging over a range of different chemical structures and chain architectures for the **T4BT-X** family. In particular, this allows us to shed new light on the literature discussion of BT torsion angles within the chain. Our experimental observations and supporting calculations indicate that changes in BT Raman intensity are seemingly not a specific signature of changes in torsion angle.

2. Results

2.1. Absorption

Figure 2 shows the absorption and normalized PL emission spectra for thin film samples of **T4BT-A**, **-B**, **-C**, **-D** and **-E** on Spectrosil B substrates. The corresponding spectra for thin film samples of **F8BT** (65 nm film) and **T4** (50 nm film) are shown in Figure 1 for reference. A number of features are immediately evident. The **T4** absorption spectrum, as previously reported,[29] closely resembles the spectrum for poly(9,9-dihexylfluorene) with two main features close to 220 and 370 nm corresponding in a simplified description to localized-localized (corresponding to feature I in Figure 2) and delocalized–delocalized (corresponding to feature II in Figure 2) (highest occupied molecular orbital (HOMO) to LUMO) π–π^* transitions of the 9,9-dihexylfluorene arms/truxene core. The alternating copolymer **F8BT** has a similar high-energy localized-localized (feature I) π–π^* transition peak near 220 nm but two longer wavelength peaks close to 330 nm and 455 nm that are understood to involve, respectively, transitions between the HOMO and higher lying delocalized unoccupied molecular orbitals (feature II) (similar to the delocalized-delocalized transition of **T4**) and between the

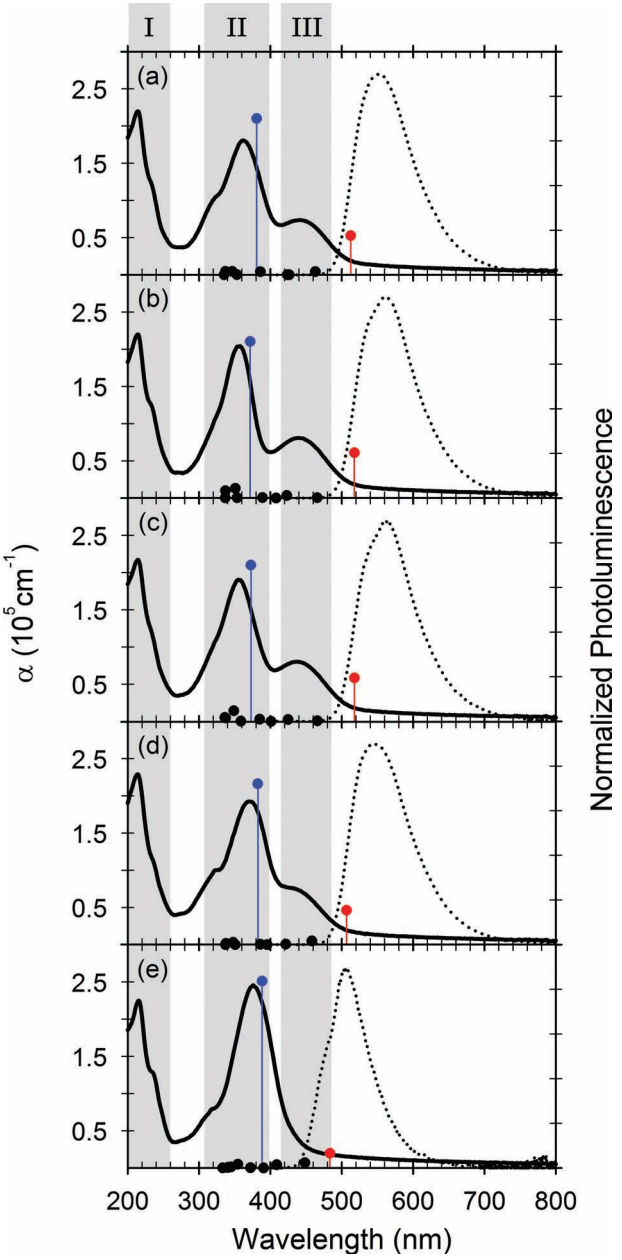

Figure 2. Absorption coefficient (α, 10^5 cm^{-1}) (solid lines, left ordinate) and normalized photoluminescence emission (dotted lines, right ordinate) spectra for thin film samples of a) **T4BT-A**, b) **-B**, c) **-C**, d) **-D** and e) **-E**. The absorption features I, II and III described in the text are highlighted by the grey shaded areas. The absorption data shown here were obtained for 50 ± 5 nm thickness films while the PL spectra were recorded for 30 ± 7 nm films in order to limit self-absorption effects. The TD-DFT calculated oscillator strengths (discrete circles data and vertical lines) for the many, low-lying optical transitions are also plotted. The oscillator strengths for transitions II and III are highlighted in blue and red respectively.

HOMO and LUMO (corresponding to feature III in Figure 2), with the LUMO now spatially localized on the BT unit.[11,28] In some respects, compounds **T4BT-A**, **-B**, **-C**, **-D** and **-E** have absorption spectra that interpolate between the two reference materials (**T4** and **F8BT**). As expected, all five compounds have the high-energy localized-localized π–π^* transition peak near 220 nm (feature I). Interestingly, however, the absorption spectrum of **T4BT-E** provides no clear evidence for the presence of BT units within the chemical structure. It has a single long wavelength peak that aligns with the 370 nm peak in **T4** (feature II), although it is slightly broadened and does show a weak short-wavelength shoulder that if present in **T4** is not so clearly resolved. We discuss this compound further below but first we focus on the other four. A closer examination of Figure 2 suggests there is a pair-wise correspondence of the spectra for (i) **T4BT-A** and **T4BT-D** and (ii) **T4BT-B** and **T4BT-C** that can be rationalized in terms of the chemical structures on the basis that the arms conjugatively couple to one effective 9,9-dihexylfluorene unit within the truxene core (highlighted in Figure 1). We then have pairs of equivalent conjugated segments comprising (i) F6′-BT-F6-F6-F6-F6 (**T4BT-A**) and F6′-F6-F6-F6-BT-F6 (**T4BT-D**) and (ii) F6′-F6-BT-F6-F6-F6 (**T4BT-B**) and F6′-F6-F6-BT-F6-F6-F6 (**T4BT-C**) where F6 signifies a 9,9-dihexylfluorene unit and F6′ the effective 9,9-dihexylfluorene unit within the truxene core. For the **T4BT-A** and **T4BT-D** pair, transitions between the HOMO and higher lying delocalized unoccupied molecular orbitals (feature II) are split into two components, a clear peak at ≈ 362 nm and 370 nm, respectively, with a well-defined shoulder at ≈ 320 nm. For the **T4BT-B** and **T4BT-C** pair, these transitions (feature II) show a peak at ≈ 356 nm with the suggestion of a shorter wavelength (unresolved) shoulder again around 320 nm. The main peak position and splitting appear to correlate with the uninterrupted lengths of F6/F6′ sequences either side of the BT unit. For the **T4BT-A** and **T4BT-D** pair we have one and four 9,9-dihexylfluorenes whereas for the **T4BT-B** and **T4BT-C** pair it is two and three—this explains both why the main peak (feature II) is more red-shifted for the **T4BT-A** and **T4BT-D** pair and the splitting, between the main peak and the shoulder, is greater. The most red-shifted peaks are found for **T4BT-E** and **T4** where there is a five F6/F6′ sequence involved in their (feature II) transitions.

The fitted peak wavelengths, λ_{III}, for the HOMO-LUMO transition III of each compound are reported in **Table 1**. For the **T4BT-A** and **T4BT-D** pair $\lambda_{III} \approx 445$ nm with an associated peak absorption coefficient (α_{III} in Table 1) 38 ± 1% that of transitions II between the HOMO and delocalized unoccupied molecular orbitals centred on F6/F6′ units. For the **T4BT-B** and **T4BT-C** pair $\lambda_{III} \approx 440$ nm with a peak absorption coefficient 41 ± 1% that of transitions II. As already noted above, in **F8BT** the HOMO-LUMO transition III is at ≈ 455 nm and has an absorption coefficient that is, if anything, marginally stronger than that of transitions II. The somewhat weaker HOMO-LUMO transition III we find for the present set of compounds is consistent with results from an earlier report on $F8_{(1-x)}BT_{(x)}$ copolymers with varying fractions of BT incorporation (x = 0.06 to 0.5).[28] The argument given there was that the HOMO-LUMO oscillator strength increases as the spatial overlap of molecular orbitals increases and hence the ≈ 17% BT conjugated structures in **T4BT-A**, **-B**, **-C**, **-D** and **-E** would indeed be expected to have weaker transitions III than the 50% BT (**F8BT**) copolymer. The anomalous behavior of **T4BT-E** in this regard, with no evident transition III, is noted again. Our multipeak fitting procedure (see the Supporting Information for details) was unable to fit a physically meaningful oscillator in the 445 nm region of the **T4BT-E** spectrum, and so we are forced to conclude that if there is a transition present here, it must have extremely small oscillator strength.

Table 1. Numerical values for selected physical properties of the **T4BT-X** family. λ_{II} and λ_{III} are, respectively, the peak wavelengths deduced from fitting transitions II and III and α_{II} and α_{III} the corresponding peak absorption coefficients; S_{II} and S_{III} are the related absorption integrals defined as $S = \int \alpha(E) dE$, where $\alpha(E)$ is the absorption coefficient (modelled as a Gaussian oscillator) and E the photon energy; $\lambda_{PL\ max}$ is the peak of the photoluminescence spectrum; Φ_{PL} ($\lambda_{II}ex$) and Φ_{PL} ($\lambda_{III}ex$) are the PL quantum yields for excitation at transitions II and III respectively; $< \tau >$ is the first temporal moment of the transient decay; $n(\lambda_{PL\ max})$ is the refractive index evaluated at $\lambda_{PL\ max}$; $\upsilon_{F6\ Ph}$ is the fitted peak wavenumber for 9,9-dialkylfluorene phenyl ring stretching; $\upsilon_{BT\ Ph}$ and $\upsilon_{BT\ C–C}$ are the fitted peak wavenumbers for BT phenyl ring stretching and C–C stretching respectively, with $A_{BT\ Ph}$ and $A_{BT\ C\text{-}C}$ the corresponding amplitudes.

Property	T4BT-A	T4BT-B	T4BT-C	T4BT-D	T4BT-E
λ_{II}[n m]	364	357	358	372	376
α_{II}[10^5c m^{-1}]	1.8	2	1.9	1.9	2.4
S_{II}[10^4 eV cm^{-1}]	7.7	7.3	7.8	8.0	11.1
λ_{III}[n m]	445	440	440	444	_
α_{III}[10^5c m^{-1}]	0.7	0.8	0.8	0.7	_
S_{III}[10^4 eV cm^{-1}]	2.4	3.2	3.0	1.9	_
$\lambda_{PL\ max}$[n m]	553	561	562	546	507
Φ_{PL}(λ_{II} ex) [%]	43 ± 4	39 ± 2	41 ± 3	41 ± 4	27 ±4
Φ_{PL}(λ_{III} ex) [%]	54 ± 7	53 ± 6	55 ± 7	52 ±6	_
$< \tau >$[n s]	3.4	3.6	3.6	4.0	3.3
n($\lambda_{PL\ max}$)	1.75	1.75	1.75	1.76	1.78
$\upsilon_{F6\ Ph}$[c m^{-1}]	1608	1608	1608	1608	1607
$\upsilon_{BT\ Ph}$[c m^{-1}]	1547	1547	1547	1547	1538
$A_{BT\ Ph}$	0.289	0.326	0.300	0.225	0.031
$\upsilon_{BT\ C\text{-}C}$[c m^{-1}]	1360	1361	1361	1362	_
$A_{BT\ C\text{-}C}$	0.086	0.101	0.080	0.080	_

2.2. Photoluminescence Measurements

As noted for the absorption spectra, there is also a pair-wise correspondence of PL spectra (Figure 2, dotted lines, excitation at λ_{II} in Table 1) for (i) **T4BT-A** and **T4BT-D** and (ii) **T4BT-B** and **T4BT-C**, although the differences between the pairs are more subtle than was the case for absorption. The **T4BT-B** and **T4BT-C** pair has the more red-shifted PL (562 nm peak) and a slightly more structured line shape with an unresolved shorter-wavelength shoulder. The **T4BT-A** and **T4BT-D** pair has an essentially featureless, weakly blue-shifted PL (553 nm and 546 nm respectively). In all four cases the PL spectra are similar to the spectrum for **F8BT**, albeit in each case somewhat blue shifted from the **F8BT** 569 nm peak. It is also noteworthy

that, unlike the case for BT-fluorene co-polymers[28] with similar BT fractions, we observe no (fluorene localized) blue light emission from either thin-film samples or solutions (data not shown) of **T4BT-A**, **-B**, **-C**, and **-D**. **T4BT-E** is again anomalous with a strongly blue-shifted PL spectrum (507 nm peak) but not possessing the vibronically structured, blue (417 nm peak) PL of **T4**. In this sense, the PL spectra more clearly reveal the difference in chemical structure between **T4BT-E** and **T4**. In addition, the observed large Stokes shift between absorption and PL emission peaks for **T4BT-E** suggests that there may be a significant geometric relaxation following excitation of this compound via transition II. Again, this is discussed in more detail below.

The subtle PL spectral changes among **T4BT-A**, **-B**, **-C**, and **-D** have essentially no effect on their PLQY values (**Figure 3**a).

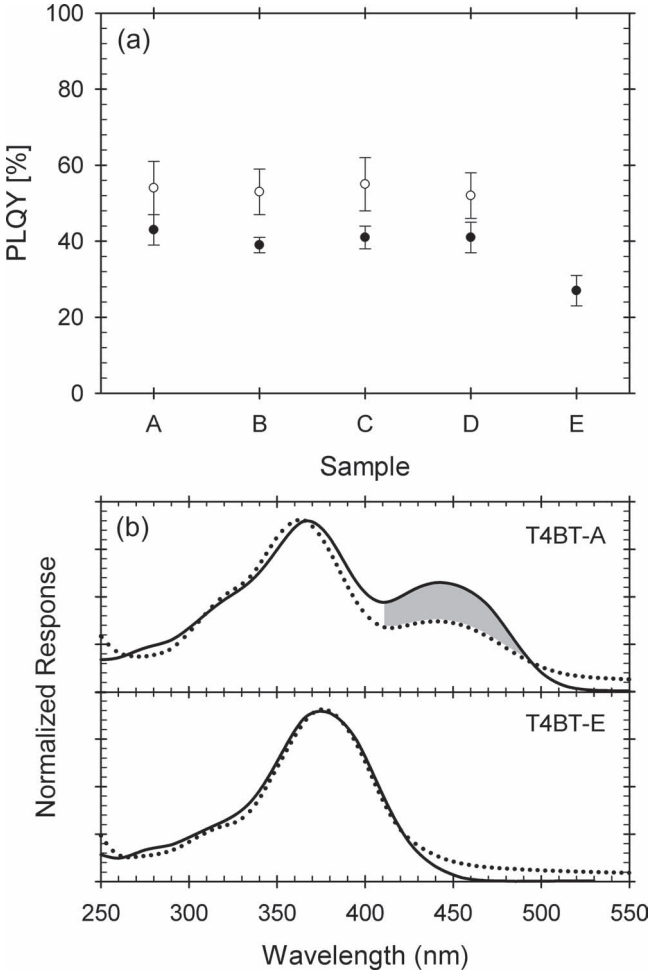

Figure 3. a) PLQY values for **T4BT-A**, **-B**, **-C**, **-D** and **-E** for excitation at transitions II (filled circles) and III (empty circles) (see Figure 2). b) Photoluminescence excitation (PLE) spectra (solid lines, peak normalized at transition II) for **T4BT-A** (600 nm PL detection, upper panel) and **T4BT-E** (550 nm PL detection, lower panel). The corresponding absorption spectra (dotted lines, peak normalized at transition II) are included for comparison. The increase in PLQY as the excitation wavelength is moved from transition II to transition III for **T4BT-A** manifests as a relative increase (shaded area) in the PLE signal strength compared to the underlying absorption.

However, as also found for **F8BT**,[30] their PLQY values do depend on which of the absorption transitions II or III is optically pumped. A higher efficiency is achieved for direct excitation at transition III (open circle data points, $\Phi_{PL} = 55 \pm 7\%$), rather than cascaded excitation via transition II (filled circle data points, $\Phi_{PL} = 40 \pm 4\%$). Figure 3b (upper panel) further shows this wavelength dependence by comparison of PLE (solid line) and absorption (dotted line) spectra; the data shown are for **T4BT-A** with peak normalization at transition II. The relative enhancement of PLE (grey shaded area) in the spectral vicinity of transition III is evident. Similar enhancements were found for **T4BT-B**, **-C** and **-D** (not shown). **T4BT-E** again stands out; this time by virtue of having a significantly lower PLQY ($\Phi_{PL} = 27 \pm 4\%$) than the other members of the **T4BT-X** family (Figure 3a) and through its PLE and absorption spectra rather closely matching each other (Figure 3(b), lower panel). The apparent long wavelength tail in the absorption spectrum of **T4BT-E** is also revealed to be most likely the consequence of scattering and/or reflection rather than true absorption since excitation at those wavelengths does not generate PL. This latter observation, taken together with the absorption peak fitting results (see the Supporting Information) supports the deduction that transition III, if present, can only be very weak for compound **T4BT-E** and/or is much more blue-shifted than theoretically predicted (*vide infra*) so that it strongly overlaps with transition II.

PL transients were measured for 50 nm thickness films of each of the **T4BT-X** compounds following 1 MHz, 70 ps pulse excitation at 405 nm. **Figure 4**a displays the data for **T4BT-D** and **T4BT-E**, representing the decay time extrema (Figure 4b). The transient for **T4BT-D** follows an almost straight-line (i.e., mono-exponential) decay when plotted, as here, on a semi-logarithmic scale. The same is true for **T4BT-A**, **-B** and **-C**, allowing us to adopt a numerical convolution approach to extract the excited state lifetime for each of these compounds. The experimental traces were best-fitted to the convolution of the recorded excitation response and a single exponential function of varying duration. The same procedure was used for the **T4BT-E** decay transient even though it is not truly mono-exponential. The deduced decay times are shown in Figure 4b. Other forms of fitting, including a statistical first moment measure, revealed the same trend with ≈ 8% or less variation in absolute values. Compared to the parent truxene **T4** ($\tau \approx 0.6$ ns) and **F8BT** alternating copolymer ($\tau \approx 2$ ns), **T4BT-A**, **-B**, **-C**, and **-D** have longer PL decay times, consistent with the reduced oscillator strength of their lowest energy optical absorption peaks (Figure 2). The pair-wise correspondence noted above for the absorption and PL spectra only partially holds for PL transients; compounds **T4BT-B** and **-C** have very similar decay times ($\tau \approx 3.6$ ns) but **T4BT-A** and **-D** do not. **T4BT-D** exhibits the slowest decay ($\tau \approx 4$ ns) of all compounds, almost 20% slower than **T4BT-A** ($\tau \approx 3.4$ ns). Both our multipeak fitting of the absorption spectra (see the Supporting Information) and DFT calculations (*vide infra*) indicate that transition III for **T4BT-D** has the lowest oscillator strength amongst **T4BT-A**, **-B**, **-C**, and **-D**, consistent with the recorded longer decay time but not quantitatively so. Further studies will be required to fully understand this behavior and would benefit from measuring the decay transients following selective excitation of transitions II and III rather than mixed excitation as here.

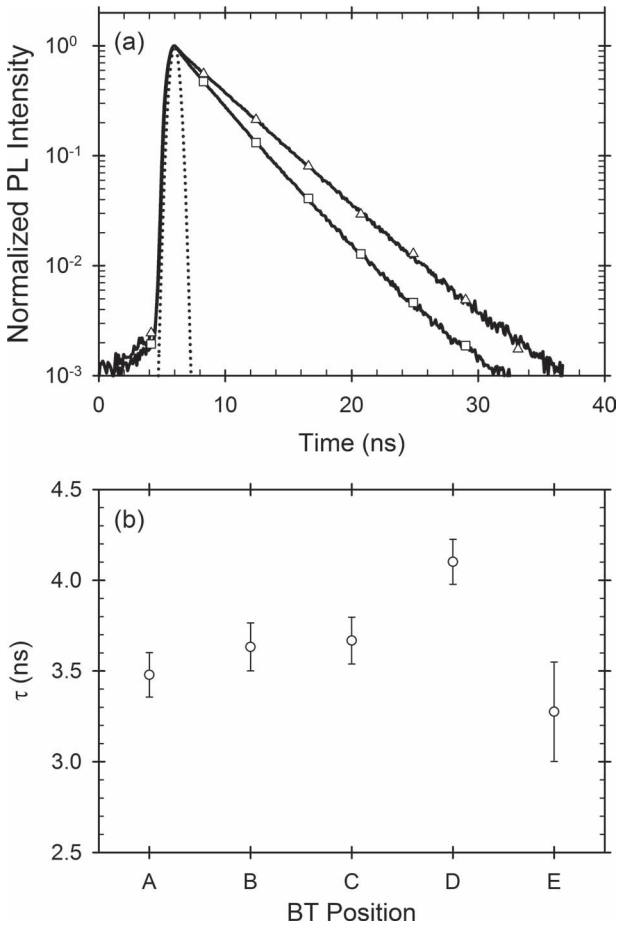

Figure 4. a) Normalized PL decay transients for **T4BT-D** (open triangles) and **T4BT-E** (open squares) under 405 nm pulsed excitation (70 ps, 1 MHz laser diode excitation). The dotted line shows the instument response function. b) Lifetimes for **T4BT-A**, **-B**, **-C**, **-D** and **-E**, extracted by fitting the convolution of a mono-exponential decay with the instrument response.

T4BT-E has the fastest ($\tau \approx 3.3$ ns) decay, consistent at first sight with PL emission following excitation via the larger oscillator strength transition II (see PLE data in Figure 3b, lower panel). However, as suggested by a lack of vibronic structure in the PL spectrum and a large Stokes shift between absorption and emission peaks, and indeed by our own TD-DFT simulations (vide infra), the emissive excited state appears to have charge transfer character and to involve a significant geometry relaxation following excitation. This plausibly explains why the decay time is longer than for the parent **T4** truxene compound despite having a lower PLQY ($\Phi_{PL} \approx 27\%$ for **T4BT-E** compared with 43% for **T4**); the transient PL further evidences the difference in chemical structure between **T4BT-E** and **T4**. Compared to the other **T4BT-X** compounds, where the variation in τ is proportionately smaller than the variation in PLQY, it is noteworthy that although **T4BT-E** has a shortened decay time, its significantly lower PLQY (Figure 3a) suggests that it may, in fact, have the longest radiative lifetime; fully consistent with a significant charge transfer character[31] and implying the importance of non-radiative decay processes, as also indicated by the non-mono-exponential decay (see Figure 4).

2.3. Theoretical Models of Electronic Structure

Density functional theory (DFT) and semi-empirical methods have been used on several occasions to study the electronic structure of linear chain molecules containing covalently linked BT and 9,9-dioctylfluorene units[11,30,32] and BT and 6,6,12,12-tetraoctylindenofluorene units.[33] The conjugated bonding interaction between 9,9-dialkylfluorene and BT moieties leads to the appearance of two main HOMO-originating optical transitions. The lowest energy of these (labelled III in Figure 2) involves a LUMO that is spatially localized on the BT unit and it is generally considered to possess a degree of charge-transfer character[28,30] though not as much as the HOMO-LUMO transition in solar cell materials wherein the BT is flanked by more strongly electron donating thiophene containing moieties.[23–26] The second (labelled II in Figure 2) links the HOMO to higher lying delocalized unoccupied molecular orbitals that are reported either to be centered on 9,9-dialkylfluorene units[11] or more fully delocalized, involving the BT unit as well.[30] This transition is similar in character to the delocalized-delocalized π–π^* HOMO-LUMO transition of **T4**[34] and poly(9,9-dialkylfluorene)s.[11]

We have undertaken further DFT/TD-DFT calculations to gain a clearer insight into the specific electronic structure of our **T4BT-X** compounds. These star-shaped molecules differ from the related linear chain **F8BT** and **F8**$_{(1-x)}$**BT**$_{(x)}$[28] copolymers in having only a single BT unit within each conjugated sequence and a precisely defined chemical structure with no polydispersity and no isomeric mixtures. Turning first to their physical structure, we find from ground state geometry optimization calculations on the proxy structures (single arm attached to truxene core with 9,9-dihydrogen rather than 9,9-dialkyl substituents for theoretical simplicity) that the torsion angle, θ, between the BT unit and its F6 neighbours is 36 ± 1^o (see Table 1) for all five of the **T4BT-X** isomers under study, an observation that has significance for the discussions presented later.

For the electronic description and following the calculation of molecular orbitals we transform to a representation based on NTOs[32] such that an occupied NTO will correspond to the state from which an electron is excited for a certain transition while a virtual NTO can be regarded as the unoccupied state to which the electron transfers. Each of the five proxy structures was modelled in turn and the results for the absorption transition intensities in the spectral range ≈ 320 – 520 nm are shown superimposed on the experimental spectra in Figure 2; calculated wavelengths and oscillator strengths of the main transitions visible are also listed in **Table 2**. Two dominant transitions corresponding to experimental peaks II and III are observed. The molecular orbitals calculated to be involved in the higher energy of these are found to be delocalized along the fluorene arm as previously found for the linear chain **F8BT** and **F8**$_{(1-x)}$**BT**$_{(x)}$ copolymer structures.[11,28,30] In the case of the lower energy peak, again there is good agreement, with the transition being one that links a delocalized HOMO (spread along the fluorene arm) to a LUMO that is spatially localized on the BT unit. This is true for all five of the proxy structures. The DFT/TD-DFT predictions of the transition wavelengths are in reasonable agreement with experiment, with 12–17 nm red shift

for transition II and 63–78 nm for transition III. The larger deviations in the latter case are understandable as our theoretical approach is less reliable for the calculation of charge transfer state energies.[33] Encouragingly the pair-wise association, first suggested from the molecular structure and measured absorption and PL spectra, between **T4BT-A** and **-D** and **T4BT-B** and **-C** also emerges clearly in the theoretical data. For example the transition II wavelengths for the **T4BT-B** and **T4BT-C** pair exhibit a blue shift compared to those found for the **T4BT-A** and **T4BT-D** pair. Furthermore, the increased separation between transitions II and III for the **T4BT-B** and **T4BT-C** pair, which as noted earlier enhances the visibility of their transition III in Figure 2, is also faithfully reproduced by the calculations.

Figure 5 shows the TD-DFT calculated probability density distributions of the occupied (blue bars) and unoccupied (red bars) NTOs associated with the lowest energy optical transition of the **T4BT-X** proxy structures (corresponding to transition III–a similar analysis of the states corresponding to transition II is available in supplementary information). The bar charts are plotted as a function of site position, moving (from left to right) away from the truxene core-based F6' site and presented so as to emphasize the pair-wise associations. Panel (a) shows the results for the **T4BT-A**/**-D** pair, panel (b) for the **T4BT-B**/**-C** pair and panel (c) for **T4BT-E**. Also shown in panel (c) is the iso-surface plot for the occupied NTO wavefunction (iso-surface values ± 0.02 shown in green/purple). The localization of the unoccupied NTO on the BT unit is evident as are the relative strengths of the overlaps between the occupied and unoccupied NTOs; weakest for **T4BT-E** and strongest for the **T4BT-B**/**-C** pair.

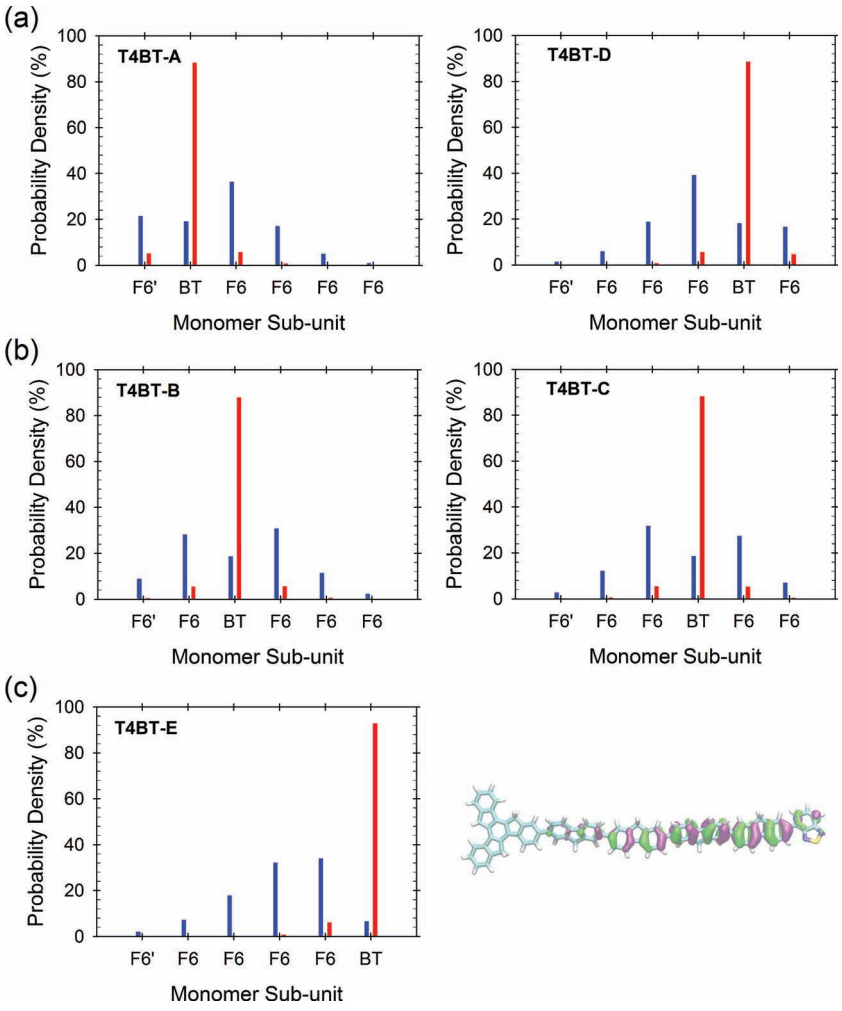

Figure 5. TD-DFT calculated probability density distributions (ground state optimized geometry) for the occupied (blue bars) and unoccupied (red bars) NTOs associated with transition III for the proxy structures of the **T4BT-X** compounds. Panel (a) shows the results for the **T4BT-A**/**-D** pair, panel (b) for the **T4BT-B**/**-C** pair and panel (c) for **T4BT-E** (Left). The iso-surface plot for the occupied NTO wavefunction (iso-surface values +/- 0.02 shown in green/purple) for **T4BT-E** is shown in panel (c) (Right) for comparison.

Additional key results for the **T4BT-E** proxy include the prediction of both a lower energy transition II and an increase in its oscillator strength in comparison to the other members of the family; both these traits are consistent with experimental observations (Figure 2 and Table 1). The expected character of transition III is also reasonably well described but with greatly reduced oscillator strength and a smaller separation from transition II compared to the rest of the **T4BT-X** series. A major factor behind this weaker transition strength is the small fraction of the occupied NTO (HOMO) residing on the BT unit compared to that found for the other **T4BT-X** compounds (see Figure 5); as a consequence the calculated overlap integral with the unoccupied NTO (LUMO), which is still localized on and around the BT unit, is significantly reduced. These calculations do not directly shed light, however, on the observed PL decay time since the weaker oscillator strength for transition III would be expected to yield a longer radiative decay time. We note however that the low PLQY for **T4BT-E** points to the importance of non-radiative decay processes following excitation of transition II. These need to be better understood.

Table 2. Parameters extracted from DFT modelling and geometry optimisation of proxy structures (Figure 1) for the **T4BT-X** family. λ'_{II} and λ'_{III} are the calculated absorption wavelengths for transitions II and III, f'_{II} and f'_{III} are the corresponding oscillator strengths (dimensionless) and θ is the torsion angle between the BT unit and adjacent F6/F6′ units. All parameters were calculated using the optimized geometry for the ground state.

Parameter	T4BT-A	T4BT-B	T4BT-C	T4BT-D	T4BT-E
λ'_{II}[nm]	381	372	373	382	388
f'_{II}	3.3	3.3	3.3	3.4	3.9
λ'_{III}[nm]	513	518	518	507	483
f'_{III}	0.8	0.9	0.9	0.7	0.3
θ[°]	35	37	37	35	36

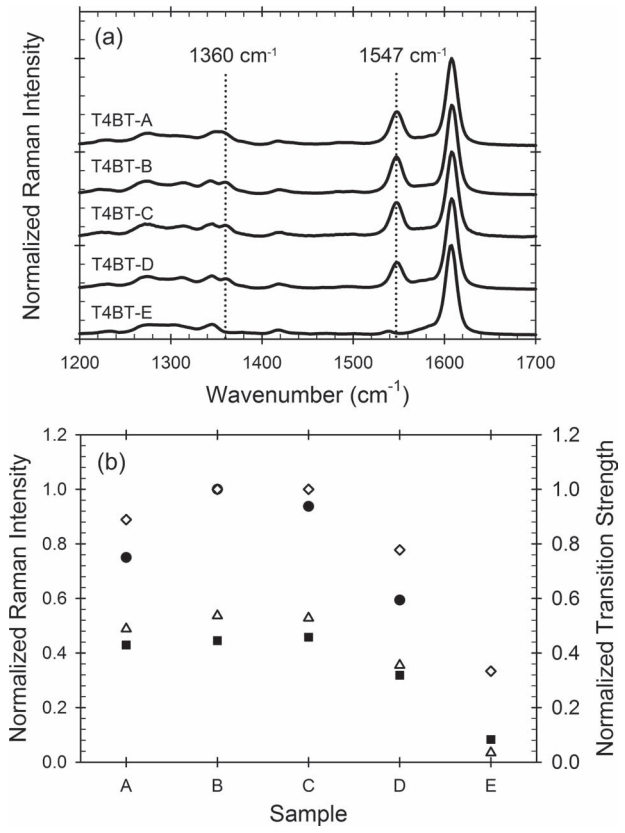

Figure 6. a) Normalized Raman scattering spectra for **T4BT-A**, **-B**, **-C**, **-D**, and **-E**. The usual BT-centred C-C (1360 cm^{-1}) and ring stretching (1547 cm^{-1}) mode frequencies are highlighted by vertical dotted lines. b) Comparison between experimental (filled squares, left ordinate) and calculated (open triangles, left ordinate) intensities for the ≈1547 cm^{-1} Raman peak for compounds **T4BT-A**, **-B**, **-C**, **-D**, and **-E**. Both data sets are normalized to the 1608 cm^{-1} 9,9-dialkylfluorene ring stretch mode intensity. The scattering cross sections were calculated using an orbital analysis on simplified proxy structures (single arm, hydrogen substituents). Also shown are the experimental (filled circles, right ordinate) integrated absorption strengths (S_{III}) and calculated (open diamonds, right ordinate) oscillator strengths (f'_{III}) of transition III for compounds **T4BT-A**, **-B**, **-C**, **-D**, and **-E** (data from Tables 2 and 3).

2.4. Raman Spectra

He-Ne laser (632.8 nm) excited Raman scattering measurements were performed for compounds **T4BT-A**, **-B**, **-C**, **-D**, and **-E** and the results are reported in **Figure 6**a. The Raman spectra are dominated by two carbon-carbon ring stretching modes at ≈ 1608 cm^{-1} and ≈ 1547 cm^{-1} and are typical of conjugated structures containing 9,9-dialkylfluorene and BT moieties with the lower wavenumber peak characteristic of BT-centered ring stretching and the higher wavenumber peak characteristic of the corresponding ring stretching for the 9,9-dialkylfluorene unit;[35–38] all other modes having substantially smaller amplitudes. The 1608 cm^{-1} peak was used for normalization since the same number of 9,9-dialkylfluorene units is present in each of the **T4BT-X** compounds. The spectra were peak fitted to determine mode magnitude and wavenumber (see results in Table 1 and SI for further details). From the fitting we observe that the **T4BT-A**, **-B**, **-C**, and **-D** compounds all share common Raman shifts for the 9,9-dialkylfluorene (1608 cm^{-1}) and BT (1547 cm^{-1}) ring stretch modes, within the nominal ± 1 cm^{-1} instrument resolution. The BT ring stretch mode softens more dramatically (by ≈ 9 cm^{-1}) to 1538 cm^{-1} for **T4BT-E**. This observation can be rationalized on the basis that the local mechanics of the BT ring stretch mode is largely unperturbed within the sequence of compounds **T4BT-A** to **-D** since each BT unit has an F6 or F6′ attached on both sides. In the case of **T4BT-E**, however, there is a 9,9-dialkylfluorene unit attached to only one side, removing a substantial restoring force and resulting in a softening of the mode. Figure 6b compares the corresponding dependence of experimental (filled squares data points) and calculated (empty triangles data points) Raman intensities for the BT ring stretch mode.

We observe that as the BT unit moves out from the core to the end of the arm (i.e., **T4BT-A** to **-E**) the Raman intensity rises slightly, peaking at the **-B**/**-C** location before falling off rapidly for the **-D** (by a factor of ≈ 1.5) and **-E** (by a factor of ≈6 theoretically and ≈13 experimentally) positions. The experimental trend is faithfully reproduced by the DFT calculations. The strength of Raman scattering depends upon the modulus squared of the equilibrium (zero displacement) polarizability gradient, $d\alpha/dr$, with α the polarizability and r the normal coordinate of the vibration.[39] Hence, whilst the polarisability gradient for the BT ring stretch mode is approximately constant for **T4BT-A**, **-B** and **-C**, it clearly falls when the BT unit is placed at positions **-D** and especially **-E**. We re-iterate that the calculations were performed with a fixed torsion angle (36 ± 1°) so changes in the calculated intensities cannot be a consequence of twisting of the BT unit relative to neighboring F6 units.

The weaker Raman scattering in the 1200–1500 cm^{-1} spectral range also depends on the BT unit position, most notably for the ≈1360 cm^{-1} peak that has previously been used to characterize the torsion angle of the **BT** unit within **F8BT**.[40] In the case of **T4BT-A** to **-E**, this peak displays a similar trend to that found earlier for the ≈ 1547 cm^{-1} BT ring stretch (Figure 6b) as perhaps might be expected given its similar BT unit[28,38] origin.

2.5. Amplified Spontaneous Emission

Amplified spontaneous emission (ASE) measurements were carried out for thin film samples of each member of the **T4BT-X** family in order to probe their ability to provide optical gain. It is worth recalling that both of the reference materials, **F8BT** and **T4** have been previously shown to provide significant optical gain, supporting amplification and lasing.[12,29] Representative results, for **T4BT-B**, are presented in **Figure 7**a. Pumping the sample with increasing incident energy causes the PL spectrum to collapse into a line-narrowed peak, typical behavior for amplified spontaneous emission. The ASE spectrum (solid line) peaks at the PL (dotted line) maximum, somewhat shorter in wavelength (561 nm) than for **F8BT** where the ASE peaks at 575 nm.[12] The power dependence of the ASE is presented in Figure 7b. The onset of a super-linear region just above ≈60 μJ cm^{-2} is coincident with the spectral width reducing to around half its initial PL value and is frequently assigned as the onset of ASE (or ASE threshold). ASE saturation is also

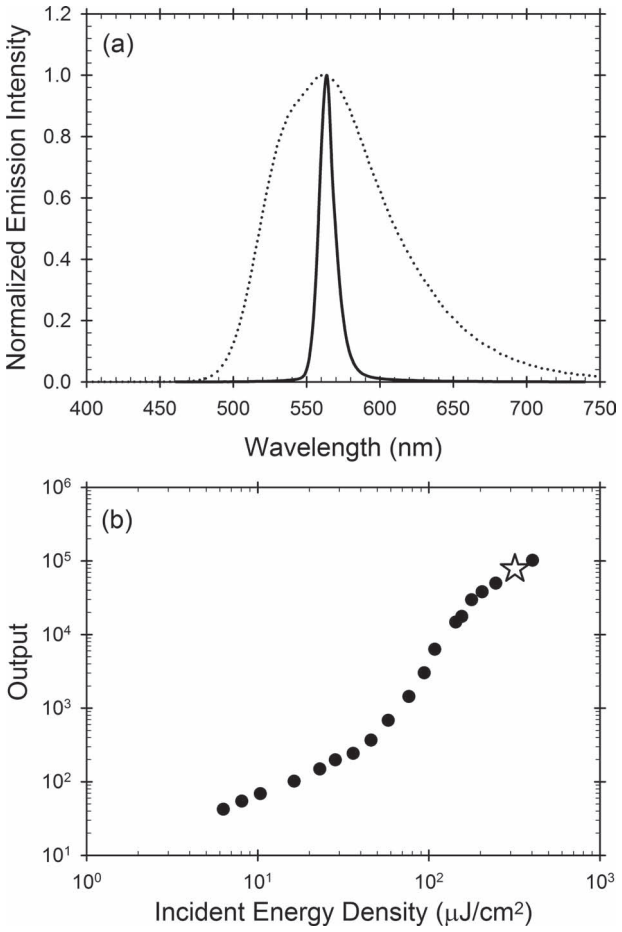

Figure 7. a) Normalized amplified spontaneous emission (ASE) spectrum (solid line) for a **T4BT-B** film (120 ± 10 nm) at an incident pump energy density of 320 μJ cm^{-2}. A normalized PL spectrum (dotted line) is also shown for reference. b) Incident pump energy density dependence of the ASE (filled circles data); the data point highlighted by a star indicates 320 μJ cm^{-2} excitation, corresponding to the ASE spectrum plotted in a).(a).

visible for pump energy densities above ≈200 μJ cm^{-2}. For comparison we note that for **F8BT** the energy density typically required for the onset of ASE is ≈40 μJ cm^{-2}. Similar results to those for **T4BT-B** were obtained for **T4BT-A**, **-C**, and **-D**. However, for **T4BT-E** there was no evidence of ASE for incident pump energy densities up to the 500 μJ cm^{-2} limit of our pump laser system. The absence of ASE in the **T4BT-E** compound is intriguing and has yet to be fully understood. The observed PLQY and emission decay time results do not obviously suggest that ASE should be absent; for comparison, blends of 20 wt% regioregular poly(3-hexylthiophene) with 80 wt% **F8BT** have similar PLQY values (Φ_{PL} ≈ 25%) and shorter decay times but still show efficient ASE and lasing.[41] PL spectra generally map the emission following excited state relaxation (Kasha's Rule)[42] and as long as the processes involved in the relaxation occur rapidly enough to not overlap in time with the emissive decay they can be largely ignored or, if competing with the formation of the emissive state, can be considered simply as part of an average non-radiative decay rate. In ASE (and lasing), however, the radiative decay time is drastically reduced due to emission stimulation and as a consequence processes involved in the excited state relaxation may then directly compete with the emission. Clearly a more detailed examination is required to unravel the likely contributing factors but we note the evidence already discussed above for significant excited state relaxation in this compound.

Table 3. Summary of experimental results characterizing the properties of **T4BT-X** compounds.

Technique	Results Summary
Absorption Spectra	• Pairwise correspondence between **T4BT-B** and **- C** and **T4BT-A** and **- D** absorption spectra. • Only transition (II) observable for **T4BT-E**.
PL Spectra	• Pairwise correspondence between **T4BT-B** and **- C** and **T4BT-A** and **- D** PL emission spectra; associated with absorption transition III. • **T4BT-E** emission appears at considerably shorter wavelength; associated with absorption transition II but showing a large Stokes shift and negligible vibronic structure in contrast to the spectra for **T4**.
PL Quantum Yields	• Similar PLQY for **T4BT-A**, **- B**, **- C**, and **- D**, with excitation at transition III exhibiting a higher Φ_{PL} value than excitation at transition II. • PLQY reduced for **T4BT-E** and only excited via transition II. • PLE spectra show consistent enhancement of transition III spectral region for **T4BT-A**, **- B**, **- C**, and **- D**.
PL Decay Transients	• Pairwise correspondence between **T4BT-B** and **- C** is preserved. • Divergence between **T4BT-A** and **- D** behaviors - qualitatively consistent with calculated weaker transition III for **T4BT-D**. • **T4BT-E** exhibits shortened, non-mono-exponential decay time.
ASE	• Amplified spontaneous emission readily observed for **T4BT-A**, **- B**, **- C**, and **- D**. • No ASE for **T4BT-E** up to 500 μJ/cm^2 pump energy density.
Raman Scattering	• All **T4BT-X** compounds have very similar Raman spectra. • Intensity of BT-centred vibrational modes increases from **T4BT-A** to **- B**, to **- C** then decreases from **T4BT-C** to **- D**, to **- E**. • Calculated Raman intensities show analogous behavior.

3. Discussion

A summary of the key experimental observations for the **T4BT-X** family of compounds is presented in **Table 3**. In an effort to focus on the positional role of the BT unit the results from each technique are discussed in terms of the pairings identified earlier through consideration of the molecular geometry (Figure 1) and supported by the calculated NTOs (Figure 5).

Considering first the basic optical properties of our materials, the pair-wise correspondence appears compelling. The three groupings, i.e., **T4BT-A/-D**, **T4BT-B/-C** and **T4BT-E**, each give rise to distinct characteristics in both absorption and PL spectra. Geometry optimized DFT/TD-DFT studies provide further support for this grouping in regard of the relative trends in (computed) transition energies. In the case of transitions between the HOMO and higher-lying delocalized unoccupied molecular orbitals (transition II region of Figure 2) we find that

those for **T4BT-B/-C** are most blue-shifted, followed by **T4BT-A/-D**, with the lowest energy arising for the **T4BT-E** structure. The trend to lower energies is entirely consistent with the size of the longest sequence of adjacent F6/F6′ units in the arm; determined by the BT unit location this ranges from 3 F6/F6′ units for **T4BT-B/-C** to 5 for **T4BT-E**. Moreover, the computed energy splitting between transitions II and III follows a similar vein (i.e., largest for **T4BT-B/-C** smallest for **T4BT-E**) and again is consistent with observations for the measured absorption spectra, e.g., the greater visibility of transition III for the **T4BT-B/-C** pair arising from a larger energy splitting.

However, not all properties mirror this behavior. Specifically, PL decay transients show a significantly different variation with BT position (see Figure 4 inset). **T4BT-B/-C** exhibit very similar decay times ($\tau \approx 3.6$ ns) i.e. they do still appear to behave as a pair but **T4BT-A** ($\tau \approx 3.4$ ns) and **-D** ($\tau \approx 4.0$ ns) are quite distinct from each other and taking into account their PLQYs to estimate their radiative decay times enhances rather than diminishes the difference. **T4BT-D** has noticeably the longest decay time of all five compounds, qualitatively consistent with its smaller calculated transition III oscillator strength (Figure 6b), albeit tempered by the excitation wavelength (405 nm) overlapping in part with transition II. **T4BT-E** has the shortest observed decay time ($\tau \approx 3.3$ ns) but this is for pumping predominantly via transition II rather than III. Transition III is expected to have much smaller oscillator strength (there is little overlap between occupied and unoccupied NTOs (Figure 5)) and is not in fact resolved as a separate peak in the absorption (Figure 2) or PLE (Figure 3b) spectra. **T4BT-E** also has a substantially smaller PLQY ($\Phi_{PL} \approx 27\%$) than the other compounds and as such may not be directly comparable - non-radiative processes clearly play a greater role for this compound (recall also its non-mono-exponential decay transient). The molecular symmetry of the arm does not therefore provide a full picture for the PL decays; the discussion needs also to consider the *absolute* placement of the BT unit within the arm. One could, for example, imagine that the tendency for BT moieties to interact with like units on neighboring molecules would depend on distance from the truxene core.

Comparison of the Raman spectra in Figure 6 also shows that whilst the position of the BT unit is still a factor, it is no longer the case that there is a strict pairing of positions; this is true for both experimental and DFT calculated scattering intensities (Figure 6b). With this in mind, we return again to the interpretation of the results from Raman spectroscopy, drawing on a number of previous studies on the **F8BT** copolymer system.

Previous Raman studies in the literature, concerned with the BT unit in the polymer **F8BT**, have generally correlated the degree of planarization of the BT and neighboring F8 units (i.e., the torsion angle between aromatic rings in the conjugated backbone tending to zero) with the relative intensities of the in-plane modes.[31,38,40] Donley *et al.*[40] reported that planarization leads to a relative decrease in the Raman intensity for the 1360 cm^{-1} BT peak and Schmidtke *et al.*[38] that the relative strength of the 1547 cm^{-1} BT ring stretching mode should increase with planarisation. Examining our data (Figure 6) we find that *both* of these modes reduce in intensity when the BT unit is moved to the **-D** position and diminish further for the **-E** position. Our observation that both peaks decrease in relative intensity as the unit moves towards the arm-end position is then seemingly at odds with the literature reports for **F8BT**, at least in respect of the proposed correlation. It is rather difficult to accept the arguments made in those publications in relation to the BT unit torsion angle in light of this behavior. Our theoretical modelling, moreover, yields the same torsion angle for the BT unit of $36 \pm 1°$ for *all* of the proxy structures. Yet these same calculations faithfully reproduce the observed reduction in the BT ring stretching mode intensity (Figure 6b); we do not need to invoke a change in torsion angle to explain the observed changes. Also shown in this graph (right ordinate) are the calculated oscillator strengths for transition (III) and the experimentally determined absorption integrals; they closely mimic the trend displayed by the Raman scattering intensities, suggesting that changes in wavefunction most likely play the major role. Reminding ourselves that geometry-optimized calculations are routinely, as here, carried out in the gas phase,[31,38,40] we should recognize that the ignored packing interactions between molecules in the solid state may well affect the absolute torsion angles. One might also imagine that such interactions would be most pronounced for BT moieties at the end of a truxene arm, i.e., **T4BT-D** and **T4BT-E** but it seems likely that any such changes do not substantially contribute to the variation in Raman intensities.

Finally, in relation to the optical gain properties of these **T4BT-X** compounds (examined via ASE studies), we find that placing the BT unit at the end of the 9,9-dialkylfluorene arms has a detrimental effect. It would be interesting to know if the same applies to linear chain alternating copolymer **F8BT**[12] and/or statistical copolymer $\mathbf{F8_{(1-x)}BT_{(x)}}$[28] samples. The detailed nature of the behavior that limits optical gain will need further investigation.

4. Conclusions

In summary, we have presented the synthesis and detailed characterization of a series of structural isomers of trigonal star-shaped molecules comprising a truxene core with quater-dialkylfluorene arms appended that contain BT moieties placed in each possible position along the arm (Figure 1: **T4BT-A**, **-B**, **-C**, **-D**, and **-E**). These compounds are, in the main, efficient green light emitters with excellent solubility and film-forming properties and good thermal stability. The optical absorption and PL spectral properties may be adequately described in terms of three different locations for the BT unit, corresponding to a **T4BT-A/-D** pair, a **T4BT-B/-C** pair and **T4BT-E**, rationalized on the basis of molecular symmetry. A more detailed description is needed, however, to explain the trends in Raman intensity for BT-centered vibrations at ≈1357 and ≈1547 cm^{-1} and in PL decay times for which **-A** and **-D** no longer behave as a pair. This is achieved by optimized geometry DFT/TD-DFT calculations of Raman scattering intensity and transition III oscillator strength that are shown to be consistent with the observed trends. The missing/very weak transition III absorption, strongly blue-shifted PL and very weak 1360 and 1547 cm^{-1} BT-centered Raman scattering intensities of **T4BT-E** can be plausibly explained as a direct consequence of the weak HOMO/occupied NTO amplitude on the BT unit at the end of the arm.

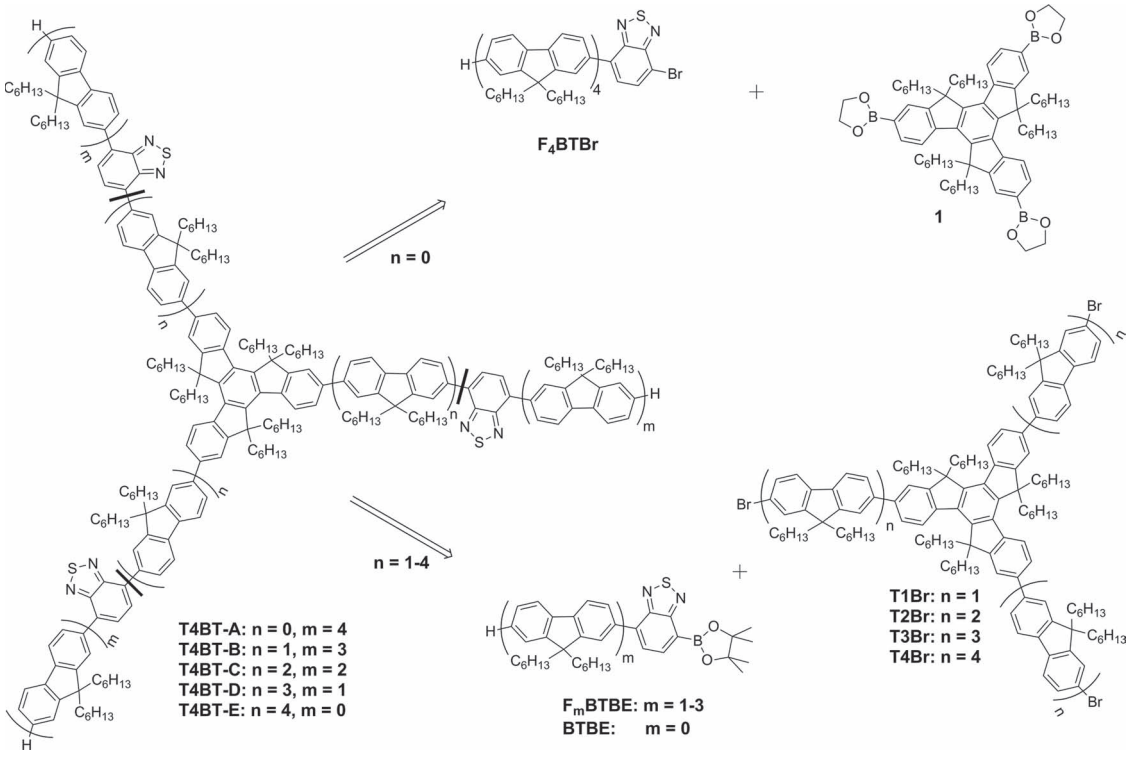

Scheme 1. Retrosynthetic scheme for the **T4BT-X** family of compounds. Bold lines represent the disconnection sites.

However, it would also appear that formation of the emissive excited state involves a fast relaxation from the Franck–Condon (vertical transition) state created by photon absorption, resulting in a low PLQY ($\Phi_{PL} \approx 27\%$) and absence of ASE when optically pumped at upto 500 μJ cm^{-2} energy density.

The precision in the chemical structure of these compounds relative to 9,9-dialkylfluorene/BT copolymers allows a consideration of the role of BT location in isolation from other factors; there is no ensemble averaging over a range of different chemical structures and chain architectures for the **T4BT-X** family. In particular, this allows us to shed new light on the literature discussion of BT torsion angles within the chain. Our experimental observations and supporting calculations indicate that changes in BT Raman intensity are not a specific signature of changes in torsion angle; any effect that alters the ground state polarisability gradient is relevant and here we tune it by proximity of the BT unit to the end of a chain.

5. Experimental Section

Synthesis: The synthetic strategy for creating the **T4BT-A** to **T4BT-E** series of C_3 symmetric star-shaped conjugated systems is presented in **Scheme 1**. To synthesize the first member (**T4BT-A**) it was found convenient to couple truxenetriboronic ester **1** with bromo(quaterdialkylfluorenyl)benzothia-diazole **F_4BTBr** for two reasons: 1) to avoid another conversion of bromide **F_4BTBr** to boronic ester and 2) to achieve a more efficient coupling by using a more electrophilic bromo-compound. The ester **1** was synthesized from tribromohexahexyltruxene **2** (see Scheme S1, Supporting Information), via lithiation with n-BuLi, followed by quenching with triisopropylborate and hydrolysis in acidic conditions. Due to the poor solubility of the polymeric anhydrous forms of the triboronic acid **2a**, the latter was converted to the ester **1**.

The other members of the series (**T4BT-B**, **T4BT-C**, **T4BT-D** and **T4BT-E**) were obtained by coupling the corresponding boronic esters **F_3BTBE**, **F_2BTBE**, **F_1BTBE** and **BTBE** with oligodialkylfluorene truxene core compounds bromo-substituted in the terminal positions, respectively **T1Br**, **T2Br**, **T3Br** and **T4Br**. We synthesized the **TnBr** compounds by bromination of the corresponding tris(oligodialkylfluorene)truxene substituted with terminal trimethylsilyl substituents **T1Si** - **T4Si** under mild conditions (0 °C, Br_2/CH_3COONa) (Supporting Information Scheme S2). Convergent and semi-convergent strategies were used for the synthesis of **T1Si** - **T3Si** and **T4Si**, respectively, using both Suzuki and Negishi coupling protocols. We found that a modified Suzuki protocol using $Ba(OH)_2$ as a base gave almost quantitative yields for **T1Si-T4Si**. To increase the yield of the oligofluorene-truxene core compounds **T1Si-T4Si** in both Suzuki and Negishi coupling protocols, it was essential to increase the equivalents of the precursor arms (boronic acid or organozinc compound) relative to the core compound **2** or **T2Br** to a ratio of 5: 1 (instead of the 3.45: 1 ratio that was used in our original publication[6]).

2,7-Dibromo-9,9-dihexyl-9H-fluorene **3** (see Supporting Information Scheme S3) was used not only for the conversion of trimethylsilylboronic acids **SiF_1B–SiF_2B** to the corresponding bromooligodialkylfluorenes of the next generation **SiF_2Br–SiF_3Br** but also as a starting compound for the synthesis of the first member of trimethylsilyl functionalized boronic acids **SiF_1B** (Supporting Information Scheme S3). In contrast to the known two-step procedure,[43] the synthesis of the latter was performed in one pot, with the following sequence: lithiation - trimethylsilylation - lithiation - boronation. Not only does this approach provide access to trimethylsilylsubstituted monobromooligodialkylfluorenes, desilylation under acidic conditions (CF_3COOH/CH_2Cl_2) quantitatively afforded monobrominated non-substituted oligodialkylfluorenes. The advantage of using compound **3** instead of monobrominated or monoiodinated 9,9-dihexyl-9H-fluorene is a much simpler approach to large-scale

synthesis, due to easier purification and handling. The synthesis of arm precursors **F_1BTBE**–**F_3BTBE** (Supporting Information Scheme S4) was performed by coupling the corresponding bromide **F_1BTBr**–**F_3BTBr** with bis(pinacolato)diboron in the presence of a weak base (CH_3COOK). Monobrominated oligodialkylfluorenylbenzothiadiazoles were synthesized by coupling of the corresponding oligodialkylfluorenyl boronic ester with a three-fold excess of dibromobenzothiadiazole **$BTBr_2$** using an anhydrous modified Suzuki protocol with K_3PO_4 as base and DMF as solvent (to provide better solubility of **$BTBr_2$**).

Each of the resulting **T4BT-A** to **T4BT-E** compounds is readily soluble in common organic solvents such as dichloromethane and dichlorobenzene. The **T4BT-A** to **T4BT-E** series also demonstrates good thermal stability. The onsets of decomposition measured by TGA are all in the temperature range 414–428 °C (Supporting Information Figure S1). DSC also reveals good morphological stability with T_g = 107–112 °C for all compounds (Supporting Information Figure S2) and no obvious crystallization. These are attractive characteristics for device application.

Sample Preparation: Thin films of the **T4BT** compounds with thicknesses 30, 50, and 120 nm (± 10% tolerance, Tencor Alphastep 200 profilometer) were spin-coated at 2000 rpm from filtered (0.2 µm Millipore), 10–40 mg/ml *o*-dichlorobenzene solutions onto pre-cleaned (10 min sonication in acetone then 2-propanol followed by 5 min, 80 W oxygen plasma exposure) Spectrosil B (quartz) substrates.

Absorption Measurements: The absorption spectra for both 50 nm and 120 nm thickness films of each **T4BT** compound were measured using a Shimadzu UV2550 spectrophotometer. Absorption coefficients were evaluated via the Beer-Lambert law and gave consistent results (within 10%) for the two film thicknesses. The corresponding refractive index spectra were derived from the absorption spectra using a Kramers-Kronig analysis[44] with reference data from a **T4** truxene sample[29] (see the Supporting Information for details).

Photoluminescence Measurements: Room temperature photoluminescence (PL) spectra were measured - using a Jobin-Yvon Fluoromax-3 spectrofluorimeter - for the 30 nm thickness films of each **T4BT** compound, thereby limiting self-absorption effects. For each material the excitation wavelength was selected to match the absorption maximum, i.e., feature II indicated in Figure 2; also see Table 1 for further details. PL Excitation (PLE) spectra were measured by recording the PL emission intensity (see Table 1 for PL maximum wavelength) as the excitation wavelength was scanned from 250 to 530 nm. PLQY measurements were performed within an integrating sphere, as described by de Mello et al.[45] with excitation performed at both absorption features II and III for **T4BT-A**, **-B**, **-C**, and **-D** and feature II only for **-E** (no significant PL was detected when exciting within the feature III wavelength range). Transient PL decay measurements used a 405 nm pulsed diode laser (1 MHz, 70 ps pulses) as excitation source, focussed onto the sample with an ×20 microscope objective. This wavelength lies between the feature II and III peaks such that absorption by both is likely to contribute to the measured dynamics. The resultant photoluminescence was collected using the same microscope objective and focussed into a Chromex 250 IS imaging spectrograph, fibre coupled to a Hamamatsu C4334 Streakscope detector. The temporal scan length was set to 50 ns and scans of 40 000 photon counts were taken at three different spatial locations on each sample; the transients reported below are averages. For each **T4BT** compound both 30 nm and 120 nm thickness films were studied with no significant variation detected in decay transient or extracted decay time.

Amplified Spontaneous Emission Measurements: 120 nm thickness **T4BT** compound films on Spectrosil B substrates were stripe-pumped (4.1 mm × 42 µm excitation area defined with a cylindrical lens) using 6–7 ns, 10 Hz, third harmonic (355 nm) pulses from a Q-switched Nd:YAG laser. The incident pump energy density was varied between 5 and 500 µJ cm^{-2} using neutral density filters inserted into the optical path. The edge-emitted, gain-guided light output was collected with a microscope objective and coupled via a liquid light guide into a spectrograph equipped with a charge-coupled device (CCD) detector.

DFT Calculations: Density functional theory (DFT) and time dependent density functional theory (TD-DFT) calculations were undertaken to gain a clearer insight into the electronic structure of the **T4BT-X** family of compounds. We used Becke's three-parameter hybrid exchange functional and Lee, Yang, and Parry's correlation functional (B3LYP) together with Pople's double zeta split basis sets (6-31g*). For computational expediency we modelled simplified proxy structures comprising a truxene core with only a single arm attached, and replaced hexyl substituents with hydrogens. We justify this approach on the basis of the C3 symmetry of the **T4BT-X** compounds and the absence of conjugation through their truxene cores. To check the consequences of this simplification we used the same methods to optimise the full structure and compared the lowest excited state energies to those of the proxies and found that they differed by less than 1%. We therefore conclude that while we expect the system to be degenerate, there is no significant effect on the molecular orbital energies. Each compound was considered in turn and the geometry in the ground state was optimized and used to compute both electronic absorption and Raman activity. Excited state calculations were carried out with TD-DFT, all others with DFT. In order to gain a clear description of the various electronic excitations we adopted a natural transition orbital (NTO) representation - obtained from diagonalizing the transition density matrix[32] - to represent the "electron" and "hole" states involved in the principal ground- and excited-state transitions.

Raman Measurements: Unpolarized Raman spectra were excited in a backscattering geometry using the 632.8 nm line of a HeNe laser focussed on the sample with a ×100 microscope objective. Spectra were collected in the 1200 to 1700 cm^{-1} range using a Renishaw micro Raman system equipped with a CCD detector. A 10 s integration time was used and the signal was averaged over 3 separate scans. After each measurement (10 mW incident power), the samples were visually inspected through the microscope to confirm that there were no signs of laser damage.

Supporting Information

Supporting Information is available from the Wiley Online Library or from the author.

Acknowledgements

We thank the UK Engineering and Physical Sciences Research Council (EPSRC) for support via the HyPix grants EP/F061609 and EP/F05999X. PNS also thanks the EPSRC for support via an Advanced Fellowship award and grant (EP/C539508 and EP/C539494). The authors further thank Emma Bailey and Ji-Seon Kim for assistance with the Raman measurements and Georges Adamopoulos for useful discussions. DDCB is the Lee-Lucas Professor of Experimental Physics.

Received: September 13, 2012
Revised: November 15, 2012
Published online: January 17, 2013

[1] M. Leclerc, *J. Polym. Sci.: Part A: Polym. Chem.* **2001**, *39*, 2867.
[2] A. Kraft, A. C. Grimsdale, A. B. Holmes, *Angew. Chem. Int. Ed.* **1998**, *37*, 402.
[3] M. T. Bernius, M. Inbasekaran, J. O'Brien, W. Wu, *Adv. Mater.* **2000**, *12*, 1737.
[4] B. K. Yap, R. Xia, M. Campoy-Quiles, P. N. Stavrinou, D. D. C. Bradley, *Nat. Mater.* **2008**, *7*, 376.
[5] E. C. C. Cheung, *Evolution of Optical Gain Properties Through Three Generations of Electroluminescent Fluorene-based Polymers*, PhD Thesis, Imperial College, London **2010**.

[6] A. L. Kanibolotsky, R. Berridge, P. J. Skabara, I. F. Perepichka, D. D. C. Bradley, M. Koeberg, *J. Am. Chem. Soc.* **2004**, *126*, 13695.
[7] Y. Wang, G. Tsiminis, Y. Yang, A. Ruseckas, A. L. Kanibolotsky, I. F. Perepichka, P. J. Skabara, G. A. Turnbull, I. D. W. Samuel, *Synth. Met.* **2010**, *160*, 1397.
[8] R. Xia, W. Y. Lai, P. A. Levermore, W. Huang, D. D. C. Bradley, *Adv. Funct. Mater.* **2009** *19*, 2844 and references therein.
[9] A. L. Kanibolotsky, I. F. Perepichka, P. J. Skabara, *Chem. Soc. Rev.* **2010**, *39*, 2695.
[10] E. P. Woo, M. Inbasekaran, W. R. Shiang, G. R. Roof, M. T. Bernius, W. Wu, US Patent, *6*, 169163, **1997**.
[11] J. Cornil, I. Gueli, A. Dkhissi, J. C. Sancho-Garcia, E. Hennebicq, J. P. Calbert, V. Lemaur, D. Beljonne, J. L. Brédas *J. Chem. Phys.* **2003**, *118*, 6615.
[12] R. Xia, G. Heliotis, P. N. Stavrinou, D. D. C. Bradley, *Appl. Phys. Lett.* **2005**, *87*, 031104 and references therein.
[13] J. Zaumseil, C. L. Donley, J.-S. Kim, R. H. Friend, H. Sirringhaus, *Adv. Mater.* **2006**, *18*, 2708.
[14] N. Tokmoldin, N. Griffiths, D. D. C. Bradley, S. A. Haque, *Adv. Mater.* **2009**, *21*, 3475 and references therein.
[15] D. Kabra, L. P. Lu, M. H. Song, H. J. Snaith, R. H. Friend, *Adv. Mater.* **2010**, *22*, 3194.
[16] C. I. Wilkinson, D. G. Lidzey, L. C. Palilis, R. B. Fletcher, S. J. Martin, X. Wang, D. D. C. Bradley, *Appl. Phys. Lett.* **2001**, *79*, 171.
[17] M. Voigt, J. Chappell, T. Rowson, A. Cadby, M. Geoghegan, R. A. L. Jones, D. G. Lidzey, *Org. Electron.* **2005**, *6*, 35.
[18] D.-Y. Chung, J. Huang, D. D. C. Bradley, A. J. Campbell, *Org. Electron.* **2010**, *11*, 1088 and references therein.
[19] P. Herguth, X. Jiang, M. S. Liu, A. K. Y. Jen, *Macromolecules* **2010**, *35*, 6094.
[20] G. Heliotis, R. Xia, D. D. C. Bradley, G. A. Turnbull, I. D. W. Samuel, P. Andrew, W. L. Barnes, *J. Appl. Phys.* **2004**, *96*, 6959.
[21] J. Huang, Q. Liu, J.-H. Zou, X.-H. Zhu, A.-Y. Li, J.-W. Li, J. Peng, Y. Cao, R. Xia, D. D. C. Bradley, J. Roncali, *Adv. Funct. Mater.* **2009**, *19*, 2978.
[22] H. Yoon, S. A. Maier, D. D. C. Bradley, P. N. Stavrinou, *Opt. Mater. Express* **2011**, *1*, 1127 and references therein.
[23] J. Nelson, *Mater. Today* **2011**, *14*, 462.
[24] M. Wang, X. Hu, P. Liu, W. Li, X. Gong, F. Huang, Y. Cao, *J. Am. Chem. Soc.* **2011**, *133*, 9638.
[25] L. Huo, J. Hou, S. Zhang, H.-Y. Chen, Y. Yang, *Angew. Chem. Int. Ed.* **2010**, *49*, 1500.
[26] H. Zhou, L. Yang, A. C. Stuart, S. C. Price, S. Liu, W. You, *Angew. Chem. Int. Ed.* **2011**, *50*, 2995.
[27] D. H. Lee, M. J. Leea, H. M. Songa, B. J. Songa, K. D. Seoa, M. Pastoreb, C. Anselmib, S. Fantacci, F. De Angelisb, M. K. Nazeeruddin, M. Gräetzel, H. K. Kimet, *Dyes Pigm.* **2011**, *91*, 192.
[28] J. M. Winfield, A. Van Vooren, M.-J. Park, D.-H. Hwang, J. Cornil, J.-S. Kim, R. H. Friend, *J. Chem. Phys.* **2009**, *131*, 035104.
[29] G. Tsiminis, Y. Wang, P. E. Shaw, A. L. Kanibolotsky, I. F. Perepichka, M. D. Dawson, P. J. Skabara, G. A. Turnbull, I. D. W. Samuel, *Appl. Phys. Lett.* **2009**, *94*, 243304.
[30] K. G. Jespersen, W. J. D. Beenken, Y. Zaushitsyn, A. Yartsev, M. Andersson, T. Pullerits, V. Sundström, *J. Chem. Phys.* **2004**, *121*, 12613.
[31] J. M. Winfield, C. L. Donley, R. H. Friend, J.-S. Kim, *J. Appl. Phys* **2010**, *107*, 024902.
[32] R. L. Martin, *J. Chem. Phys.* **2003**, *118*, 4775.
[33] Y. W. Soon, T. M. Clarke, W. Zhang, T. Agostinelli, J. Kirkpatrick, C. Dyer-Smith, I. McCulloch, J. Nelson J. R. Durrant, *Chem. Sci.* **2011**, *2*, 1111.
[34] N. A. Montgomery, J.-C. Denis, S. Schumacher, A. Ruseckas, P. J. Skabara, A. Kanibolotsky, M. J. Paterson, I. Galbraith, G. A. Turnbull, I. D. W. Samuel, *J. Phys. Chem. A* **2011**, *115*, 2913.
[35] A. Dreaw, M. Head-Gordon, *J. Am. Chem. Soc.* **2004**, *126*, 4007.
[36] M. Ariu, D. G. Lidzey, M. Lavrentiev, D. D. C. Bradley, *Synth. Met.* **2001**, *116*, 217 and references therein.
[37] H. Liem, P. Etchegoin, K. S. Whitehead, D. D. C. Bradley, *Adv. Funct. Mater.* **2003**, *13*, 66 and references therein.
[38] J. P. Schmidtke, J.-S. Kim, J. Gierschner, C. Silva, R. H. Friend, *Phys. Rev. Lett.* **2007**, *99*, 167401.
[39] P. Larkin, *Infrared and Raman Spectroscopy: Principles and Spectral Interpretation*; Elsevier, Amsterdam **2011**.
[40] C. L. Donley, J. Zaumseil, J. W. Andreasen, M. M. Nielsen, H. Sirringhaus, R. H. Friend, J.-S. Kim, *J. Am. Chem. Soc.* **2005**, *127*, 12890.
[41] R. Xia, P. N. Stavrinou, D. D. C. Bradley, Y. Kim, *J. Appl. Phys.* **2012**, *111*, 123107.
[42] M. Kasha, *Discuss. Faraday Soc.* **1950**, *9*, 14
[43] M. Tavasli, S. Bettington, M. R. Bryce, H. A. Al Attar, F. B. Dias, S. King, A. P. Monkman, *J. Mater. Chem.* **2005**, *15*, 4963.
[44] P. N. Stavrinou, G. Ryu, M. Campoy-Quiles, D. D. C. Bradley, *J. Phys.: Condens. Matter* **2007**, *19*, 466107.
[45] J. C. deMello, H. F. Wittmann, R. H. Friend, *Adv. Mater.* **1997**, *9*, 230.